Fiber Bragg Grating with Polyimide–Silica Hybrid Membrane for Accurately Monitoring Cell Growth and Temperature in a Photobioreactor

ARTICLE *in* ANALYTICAL CHEMISTRY · AUGUST 2014

Impact Factor: 5.64 · DOI: 10.1021/ac502417a · Source: PubMed

4 AUTHORS, INCLUDING:

NB Zhong
Chongqing University of Technology
19 PUBLICATIONS **47** CITATIONS
SEE PROFILE

Xun Zhu
Sun Yat-Sen University
162 PUBLICATIONS **1,453** CITATIONS
SEE PROFILE

analytical chemistry

Article

pubs.acs.org/ac

Fiber Bragg Grating with Polyimide–Silica Hybrid Membrane for Accurately Monitoring Cell Growth and Temperature in a Photobioreactor

Nianbing Zhong,*[,†] Qiang Liao,*[,‡] Xun Zhu,[‡] and Mingfu Zhao[†]

[†]School of Optoelectronic Information, Chongqing University of Technology, Chongqing 400054, China

[‡]Key Laboratory of Low-grade Energy Utilization Technologies and Systems, Chongqing University, Ministry of Education, Chongqing 400030, China

Supporting Information

ABSTRACT: A microstructured fiber Bragg grating (MSFBG) was created to accurately and simultaneously monitor the cell growth of photosynthetic bacteria (PSB) *Rhodopseudomonas palustris* CQK 01 and the temperature in a photobioreactor. The proposed sensor was made from an FBG unit that was separated into three regions, an unperturbed region, and two etched regions with smooth surfaces. The unperturbed grating region was employed to monitor the temperature. To eliminate the effects of the liquid concentration and temperature on the biomass, a polyimide–silica hybrid membrane was created and coated on an etched grating region to separate the liquids from the PSB; that is, this thinned region was developed to analyze the liquid concentration and temperature. Another etched grating region with a smaller diameter was used to determine the response to the temperature, biomass, and liquid concentration. In addition, two models were also presented to demonstrate accurate simultaneous measurement of the biomass and temperature. We discovered that the MSFBG sensor can rapidly and accurately determine the difference in the Bragg wavelength shifts caused by changes in the temperature, biomass, and liquid-phase concentration. The measured biomass is highly correlated with the real cell growth, with a correlation of 0.9438; the hydrogen production rate and temperature difference from metabolic heat production reached 1.97 mmol/L/h and 2.8 °C, respectively, in the PSB culture.

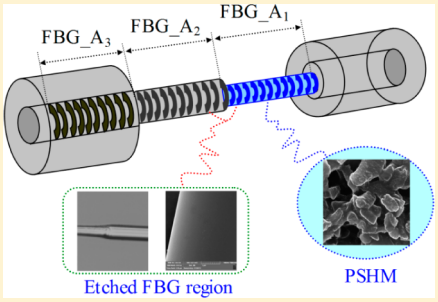

Online monitoring is an important process indicator for various industries. Effective and advanced methods of monitoring are required to develop and maintain processes at the maximum efficiency and desired product quality.[1] For example, in the chemical industry, safe process operation and product improvement result from systematic monitoring of the process variables.[2,3] In the water industry, water circuits that employ advanced applications of effective monitoring methods can reduce the environmental impact of biocide use for the control of biofilm formation and produce high-quality fresh water.[4] In the bioenergy industry, monitoring methods are also necessary to obtain a high conversion efficiency, yield, and purity of the products.[5,6] In particular, in biohydrogen technology, biological hydrogen production by free photosynthetic bacteria (PSB), such as the *Rhodopseudomonas capsulata* strain, is regarded as a promising technology because it is cost-effective and pollution-free and produces high-purity yields.[7] However, the hydrogen production efficiency is low because the biochemical conversion process lacks online monitoring and control of the cell growth, temperature, light intensity, substrate concentration, pH, and hydraulic retention time of the substrates.[8,9] Thus, efficient monitoring and quantification of the bioprocess parameters are highly important for improving the production rate and yield.[10]

The hydrogen production performance in a suspension culture is determined primarily by the biomass concentration (cell growth rate) and temperature. A low biomass concentration will cause long lag times and slow fermentation rates, whereas a high concentration may adversely affect the fermentation yields and rates.[11] Kargi et al.[12] discovered that the hydrogen yield and H_2 formation rate were affected by the biomass concentration; the specific H_2 production rate decreased when the biomass concentration exceeded an optimal level (0.48 g/L). A high biomass concentration reduces the hydrogen production levels because more toxic chemicals are generated, that is, because of product inhibition (increases in the dissolved hydrogen concentration and small organic molecules) and the limits on the substrate and illumination intensity in the fermentation environment.[13] Furthermore, in addition to the biomass concentration, the temperature has been a primary focus of bioprocess development. A suitable temperature can enhance the cell growth rate and metabolic activity because cell activity is significantly affected by the temperature and is inhibited when the environmental temper-

Received: July 1, 2014
Accepted: August 28, 2014
Published: August 28, 2014

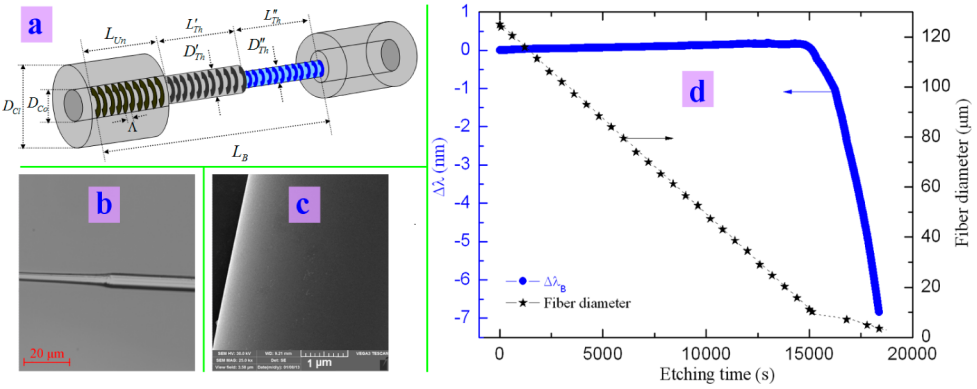

Figure 1. (a) Configuration, (b, c) surface morphology, and (d) etching properties of FBG.

ature is not suitable for cell growth.[14] Actually, the temperature information for a cell culture can also reflect the cell metabolic activity, that is, through the difference between the environmental temperature and the internal temperature of the bioreactor, which arises from metabolic heat production in the culture.[15] Hence, online acquisition of information on the biomass concentration and temperature in the cell culture process is very important for understanding and optimizing bioprocesses and improving bioreactor performance.

To realize online measurement and control of the biomass concentration in biochemical processes, many sensors using technologies such as electrical impedance spectroscopy, dielectric spectroscopy, infrared spectroscopy, optical density measurement, and fluorescence spectroscopy have been designed.[16−19] Of these methods, fiber-optic sensors have attractive properties because of their microstructure, corrosion resistance, immunity from electromagnetic interference, fast response speed, good biocompatibility, and easy installation. Thus, fiber sensors are suitable for application in the long term operation of bioreactors to obtain accurate information on cell growth.[10] Unfortunately, fiber sensors are difficult to use in practice because the obtained information is affected by the biomass (biomass denotes the dry weight of the living organisms per unit volume in the photobioreactor), temperature, and liquid-phase concentration and composition. As we know, in the cell culture process, not only the biomass but also the temperature and liquid-phase concentration and composition will change with cell growth and metabolism. Thus, it is difficult for traditional fiber sensors to distinguish the effect of various factors (biomass, liquids (liquids denotes the substrate and product in the photobioreactor), and temperature) on the biomass by measuring only the output signal. Fiber Bragg grating (FBG) sensors can be used to distinguish and monitor the solution concentration and temperature, allowing the responses to the two parameters to be isolated simultaneously.[20,21] However, it is difficult to accurately and simultaneously monitor the biomass and temperature using the designed FBG sensors. We know that the concentration measurement principle of FBG sensors is based on the refractive index (RI) change of the surrounding medium.[22,23] The RI changes with changes in the biomass and liquid-phase concentration in the cell culture. Thus, the major obstacle to accurate simultaneous measurement of the biomass and temperature is separating and quantifying the cells, liquids, and temperature.

In this work, to separate the effects of various factors (biomass, liquids, and temperature) on the sensor output signal and to accurately monitor the biomass and temperature in a culture, we propose a novel microstructured FBG (MSFBG) sensor. The MSFBG includes three regions: the temperature-sensing region, temperature- and liquid-phase-sensing region, and temperature-, liquid-, and biomass-sensing region. The latter two regions, which have smooth surfaces, were prepared to the desired diameters by wet etching to improve the Bragg reflection wavelength. Furthermore, to separate the PSB cells and liquids, a hydrophilic polyimide−silica hybrid membrane (PSHM) was also created and coated on the fiber surface of the liquid-sensing region to determine the liquid concentration and temperature. The offline performance of the proposed sensor was studied by measuring different biomass and liquid concentrations and temperatures. Online measurement of the biomass and temperature using the sensor was investigated in a culture of the PSB *R. palustris* CQK 01. We also developed models to demonstrate the simultaneity and accuracy of the measurement.

MATERIALS AND METHODS

Configuration of the MSFBG Sensor. The MSFBG sensor with three regions, an unperturbed region and two thinned regions (Figure 1a), was made from a normal FBG unit with a core diameter D_{Co} of 8.3 μm, cladding diameter D_{Cl} of 125 μm, grating pitch Λ of 535.85 nm, length L_B of 10 mm, and central wavelength of 1549.925 nm. The length of the unperturbed region, L_{Un}, was 2 mm. The length L'_{Th} and diameter D'_{Th} of one of the thinned regions were 4 mm and 7.1 μm, respectively; the other thinned region had a length L''_{Th} and smallest diameter D''_{Th} of 4 mm and 4.5 μm, respectively. For the thinned regions, to obtain a high-quality FBG reflection spectrum, a thinned grating region with a smooth surface is essential. If the prepared FBG sensing region has a rough surface, we will observe a large number of irregular Bragg reflection peaks, and a significant Bragg reflection peak will not appear, for the following reasons. First, the roughness (pits) will cause differences in the RI of the etched FBG because the employed FBG is a graded-index multimode silica optical fiber; the RI of the etched-fiber core at a radius r, n_r, can be expressed as $n_r = n_{max}[1 - (((n_{max}^2) - (n_c^2))/(n_{max}^2))(r/R)^r]^{1/2}$, where n_{max} is the RI of the fiber core axis (i.e., at $R = 0$), n_c is the RI of the fiber cladding, and R is the radius of the fiber core ($r < R$). Second, the surface roughness in the fiber's etching region increases the light scattering, refraction loss, and local difference in the modal dispersion, decreasing the effectiveness of the optical signal transmission and Bragg reflection waveguides.[24] Thus, to obtain a smooth surface on the thinned FBG, wet

dx.doi.org/10.1021/ac502417a | Anal. Chem. 2014, 86, 9278−9285

etching technology was adopted in this work, and the thinned FBG sensing regions were prepared following the literature.[25,26]

During the etching process, the jacket of the FBG region was removed, and the nonetching FBG region was coated with candle oil; thereafter, the unclad fiber (8 mm) was rapidly etched to a diameter of about 10.5 μm using hydrofluoric acid (HF, percentage concentration at 20%) at 20 °C. The etched diameter and variation in the Bragg wavelength shift are shown in Figure 1d. Next, the HF was replaced by an improved etchant, buffered hydrofluoric acid (HF/ammonia–water mixture), with pH 5.34, and an etched fiber with a diameter of 10.5 μm was continuously etched to a diameter of 7.1 μm at the same temperature. Then a 4 mm length of the etched region was coated with candle oil, and the remaining 4 mm, with a diameter of 7.1 μm, was further etched to the desired diameter of 4.5 μm. Finally, the coated candle oil was dissolved using absolute ethyl alcohol at 40 °C. The surface morphology of the etched FBG regions and a scanning electron microscopy (SEM) image of the smallest-diameter etched FBG are shown in Figure 1b,c, respectively.

To separate the liquids from the biomass (PSB), a porous hydrophilic PSHM was developed on the basis of sol–gel organic–inorganic hybrid technology proposed because of its excellent thermal stability, chemical resistance, mechanical properties, dielectric properties, and optical transparency.[27,28] The porous membrane preparation process included the following four steps: in step one, a solution of polyamic acid (PAA, polyimide precursor) and dimethylformamide was prepared using the reagents pyromellitic anhydride, *p*-phenylenediamine, and *N*,*N*-dimethylformamide.[29] In step two, silica sols were prepared as follows: at 40 °C under ultrasonic agitation at 360 W, 26.7 mL of tetraethyl orthosilicate (TEOS) was dropped slowly into 190 mL of absolute ethyl alcohol and stirred continuously for 30 min; then 4 mL of HCl (38 wt %) was mixed with 10 mL of deionized water, and the mixed solution was dropped at a rate of 0.04 mL/min into the uniform TEOS-ethanol mixture solution. The transparent, light blue silica sol was aged at room temperature for 7 days; we call the result sol A. Next, 5 mL of 3-(trimethoxysilyl) propyl methacrylate was added dropwise to 50 mL of sol A for 60 min; the result is called sol B. In step three, homogeneous PAA–silica hybrid sols were obtained as follows: 5 mL of sol B was dropped slowly into 25 mL of the PAA solution and continuously reacted for 180 min at 25 °C under ultrasonic agitation at 360 W. In step four, the PSHM was prepared as follows. Lens cleaning paper was chosen as the support material because it shows good flexibility, hydrophilicity, and porous structure.[30] The prepared PAA–silica hybrid sol was sprayed by an airbrush (HD-130, Taiwan) onto the surface of the selected paper (the prepared sol was not directly coated on the etched fiber surface because the resulting uneven distribution of the coating material causes differences in the surface RI of the FBG etched region, which disrupt the Bragg reflection). The sprayed paper was then dried in a clean room for 2 days. These two processes were performed three times. The paper was then dried in a vacuum oven at 260 °C for 240 min at a heating rate of 0.5 °C/min. The surface morphology of the proposed membrane obtained by SEM is shown in Figure 2a. The SEM image indicates that the prepared PSHM formed a porous membrane (average thickness and hole diameter of 80 and 0.32 μm, respectively). Furthermore, to compare the pore diameters of the prepared PSHM and the size of the PSB CQK 01 strain, a PSB cell was examined by an electron microscope; a negative staining electron microscopic image is shown in Figure 2b. A comparison of Figure 2a, b reveals that the fabricated membrane can be used to separate the PSB from the bacterial suspension because the PSB are far larger than the PSHM pores (normal cells have an average length of 4.3 μm and diameter of 2.2 μm).

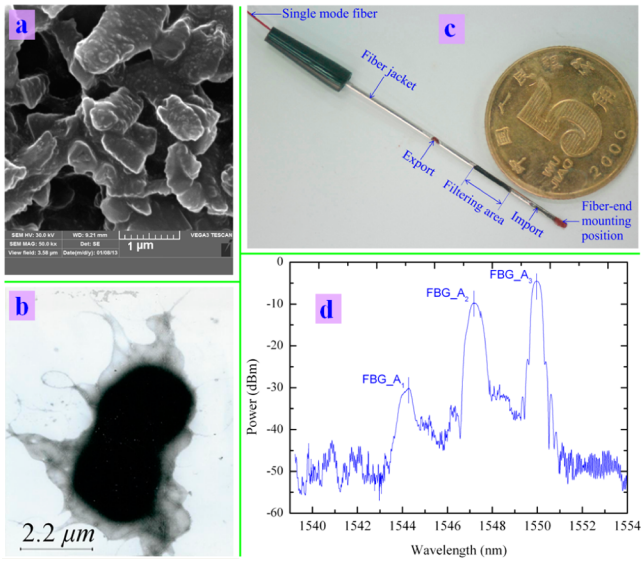

Figure 2. Images of (a) PAA–silica membrane, (b) *R. palustris* CQK 01 (PSB), and (c) packaged MSFBG sensor and (d) spectra of fabricated sensor [diameter and edge thickness of coin (RMB Wu Jiao) are 20.50 and 1.65 mm, respectively].

The MSFBG sensor was encapsulated using an approximately 35 mm long stainless steel capillary (inside and outside diameters of 200 and 500 μm, respectively). Both ends of the grating were fixed on the capillary wall using epoxy (353ND), and the three regions of the prepared sensor were separated using silicone glass with the assistance of a capillary (100 μm inside diameter) and a Keyence VHX-600 K digital microscope. The three holes (Figure 2c) in the wall of the capillary act as the solution inlet port, filter membrane assembly point, and solution outlet port, respectively. The prepared PSHM was fixed on the capillary inner wall using the epoxy and attached to the surface of the etched FBG (liquid-concentration-, and temperature-sensing region, see Figure 1a) with a diameter of 7.1 μm. Figure 2c,d show an image of the prepared MSFBG sensor and its reflection spectra in distilled water at 25 °C, respectively. The differences between the peak wavelengths of the thinned grating parts and that of the unperturbed grating part were 2.7 and 5.6 nm for the FBG regions with diameters of 7.1 and 4.5 μm, respectively. In Figure 2d, the peak wavelengths of FBG_A_1, FBG_A_2, and FBG_A_3 came from the etched FBG with a diameter of 4.5 μm, the thinned FBG with a diameter of 7.1 μm, and the unperturbed (normal) region with a diameter of 125 μm, respectively. In this work, FBG_A_1, FBG_A_2, and FBG_A_3 were used to sense the biomass and the liquid (substrate and product) concentration and temperature, the liquid concentration and temperature, and the liquid temperature, respectively.

Microorganism and Cultivation. The CQK 01 strain of the PSB *R. palustris* was employed and cultivated anaerobically with argon gas at 30 °C for 96 h under illumination from a 590 nm light-emitting diode (LED) at 4000 lx. The synthetic medium was the same as in our previous work,[13] except that the

dx.doi.org/10.1021/ac502417a | *Anal. Chem.* 2014, 86, 9278–9285

glucose concentration was adjusted to 15 g/L to facilitate cell growth and metabolism. The initial pH value of the medium before incubation was adjusted to 7.0 using NaOH solution.

Systems and Operations. Figure 3 shows a schematic illustration of the PSB culture and measurement systems. The

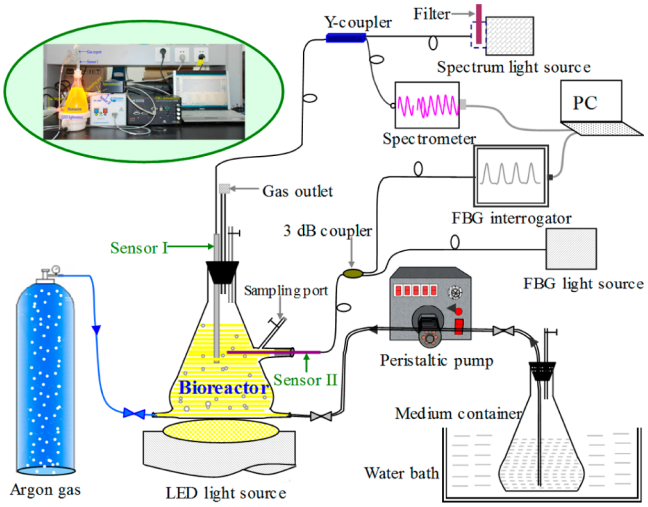

Figure 3. Schematic diagram of experimental system (sensor I is a fiber-optic sensor based on spectral measurement of the absorption; sensor II is the prepared MSFBG sensor).

photobioreactor was constructed using a 250 mL Buchner flask. Ar gas was sprayed in a continuous mode with a gas flow rate of 6 mL/min. Agitation of the Ar gas provided an anaerobic environment for the cell culture; inhibited adherent growth; prompted the uniform distribution of the cells, substrate, and product in the bioreactor; and reduced the partial pressure of biohydrogen in the reactor vessels to improve the cell culture performance. The LED light source (590 nm, 4000 lx) was mounted on the underside of the bioreactor. The MSFBG measurement system for online monitoring of the biomass and temperature consists of the prepared MSFBG sensor, full spectral scanning (1510−1590 nm) equipment, and an FBG interrogator (SM125−500, Micron Optics Inc.) with high accuracy (1 pm). Furthermore, to compare the biomass measured using the MSFBG sensor with the actual biomass, a fiber-optic sensor (Sensor I) calibrated using the relation between the absorption intensity at 600 nm and the biomass dry weight was employed. For the Sensor I measurement system, the light source (DH-2000, Ocean Optics, USA) consisted of deuterium tungsten halogen sources (deuterium lamp, 25 W and tungsten halogen lamp, 20 W) operating in the 190−2000 nm range; a broad-bandpass filter was used to admit only light between 410 and 1100 nm (LPF-400-01, DaHeng Optical Thin Film, China). The absorbed light intensity was measured with an optical spectrometer (QE65000, Ocean-optics, USA) with a spectral resolution of 0.14−7.7 nm at 400−1150 nm. Before the experiments, to prevent the introduction of other strains, the bioreactor and pipes were autoclaved at 121 °C for 15 min, and the sensor was completely sterilized with formalin for 15 min and then thoroughly washed with deionized water. Next, the prepared PSB bacterial suspension was pumped into the bioreactor under anaerobic conditions.

Measurement Principle. In normal optical fibers with an effective RI of n_{eff}, the fundamental mode is practically independent of the RI of the medium surrounding the cladding. However, when the cladding diameter is uniformly reduced, n_{eff} will depend on the external RI (ERI). In this work, an FBG unit with one unperturbed part and two thinned portions of the grating region was designed, as shown in Figure 1. The unperturbed region is used to sense the temperature, and the thinned grating regions are used to respond to the RI and temperature changes of the surrounding medium. For the unperturbed region and the thinned regions, the Bragg wavelengths can be expressed as

$$\lambda_U = 2\cdot n_{effU}\Lambda \tag{1a}$$

$$\lambda_{Th} = 2\cdot n_{effTh}\Lambda \tag{1b}$$

where λ_U and λ_{Th} are the Bragg wavelengths, and n_{effU} and n_{effTh} are the effective RIs of the unperturbed and thinned grating regions, respectively. The sensitivities of the MSFBG sensor, in terms of the wavelength shift, are given by eq 2, where α is the thermal expansion coefficient of the adopted fiber, assuming the same value for the three grating regions.[31]

$$\frac{\Delta\lambda_U}{\lambda_U} = \left(\frac{1}{n_{effU}}\frac{\Delta n_{effU}}{\Delta T} + \alpha\right)\Delta T \tag{2a}$$

$$\frac{\Delta\lambda_{Th}}{\lambda'_{Th}} = \left(\frac{1}{n_{effTh}}\frac{\Delta n_{effTh}}{\Delta T} + \alpha\right)\Delta T + \left(\frac{\Delta n_{effTh}}{n_{effTh}}\right)_{\Delta ERI} \tag{2b}$$

Obviously, the rate of change of the Bragg wavelength for the unperturbed region is sensitive only to surrounding temperature changes according to eq 2a, whereas the rate of change of the wavelength for the thinned regions (eq 2b) would respond to changes in the temperature and ERI. In particular, the Bragg wavelength shift induced by ERI changes in the thinned part is directly related to the dependence of the effective refractive index n_{eff} of the fundamental mode on the ERI and the diameter and roughness of the thinned FBG region. For a given FBG unit, when the diameter and roughness of the thinned FBG region are known, the Bragg wavelength shift will depend only on the ERI changes. However, in this work, the ERI is a complex refractive index that depends on the conditions of the bacterial suspension, that is, the biomass and liquid-phase conditions (composition and concentration of substrate and products). Actually, during the bacterial culture process, the biomass and metabolite concentration increase, whereas the substrate concentration decreases. Thus, in this work, the bacterial suspension was separated into biomass and liquid-phase components to reduce the complexity of its composition. The ERI of the bacterial suspension was described using the Lichtenecker equation under constant temperature, which is a mixing rule that is frequently used in the analysis of the RI of mixtures; n_{eff} can be expressed as follows:[32]

$$\ln n_{effTh} = \phi_1 \ln n_b + \phi_2 \ln n_{sp} \tag{3}$$

where n_b and n_{sp} are the RIs of the components, that is, the biomass and liquid phase, respectively, and ϕ_1 and ϕ_2 are the volume fractions in the bacterial suspension of the two components. The change in the wavelength is known to occur through the interaction of the evanescent field with the bacterial suspension; thus, the thinned region will respond to the biomass, liquid-phase concentration, and temperature.

To accurately and simultaneously monitor the biomass and temperature in the PSB culture process, three types of experiments should be conducted to separate the effects of the parameters, that is, the temperature, biomass, and liquid

dx.doi.org/10.1021/ac502417a | Anal. Chem. 2014, 86, 9278−9285

phase, on the rate of change of the wavelength. Thus, first, for the prepared MSFBG sensor, one should examine the changes in the wavelength with respect to the change in temperature in distilled water and the wavelength shift with respect to the changes in the concentrations of solutions (such as a glucose solution) at constant temperature. Using the experimental data, the matrix can be expressed as

$$\begin{bmatrix} \Delta\lambda_{B,2} \\ \Delta\lambda_{B,3} \end{bmatrix} = \begin{bmatrix} k_{2x} & k_{2t} \\ k_{3x} & k_{3t} \end{bmatrix} \begin{bmatrix} \Delta x \\ \Delta t \end{bmatrix} \quad (4)$$

where $\Delta\lambda_{B,2}$, k_{2x}, and k_{2t} denote the variation in the central wavelength, solution sensitivity coefficient, and temperature sensitivity coefficient, respectively, of the unperturbed region of the MSFBG sensor; $\Delta\lambda_{B,3}$, k_{3x}, and k_{3t} denote those of the thinned region of the MSFBG sensor with a diameter of 7.1 μm (see Figure 1); and Δx and Δt denote the changes in the solution concentration and temperature, respectively.

Second, one should obtain the matrix by checking the changes in the wavelength with respect to the change in the temperature in distilled water and the wavelength with respect to changes in the bacterial suspension at constant temperature. The obtained matrix can be written as

$$\begin{bmatrix} \Delta\lambda_{B,1} \\ \Delta\lambda_{B,3} \end{bmatrix} = \begin{bmatrix} k_{1y} & k_{1t} \\ k_{3y} & k_{3t} \end{bmatrix} \begin{bmatrix} \Delta y \\ \Delta t \end{bmatrix} \quad (5)$$

where $\Delta\lambda_{B,1}$, k_{1y}, and k_{1t} denote the variation in the central wavelength, bacterial suspension sensitivity coefficient, and temperature sensitivity coefficient, respectively, of the thinned region of the MSFBG sensor with a diameter of 4.5 μm (see Figure 1); k_{3y} and k_{3t} denote the bacterial suspension sensitivity coefficient and temperature sensitivity coefficient, respectively, of the unperturbed region of the MSFBG sensor; and Δy denotes the change in the bacterial suspension concentration.

By using matrices 4 and 5, one can obtain the temperature and bacterial suspension concentration, but not the actual biomass in the bacterial suspension. The reason is that, as described in eq 3, the change in the wavelength in the thinned region is affected by the biomass and liquid-phase concentration of the bacterial suspension even at constant temperature. Thus, when the thinned region of the MSFBG sensor is immersed in the bacterial suspension, the change in the wavelength is a function of the RIs of the biomass, n_b, and of the liquid phase, n_{sp}, and can be expressed as

$$\lambda_B = \lambda_B(\phi_1 n_b, \phi_2 n_{sp}) \quad (6)$$

To separate the effects of the biomass and liquid-phase concentration on the central wavelength and to accurately measure the biomass in a culture, eq 6 is processed by applying the Taylor expansion and using only the first terms of the Taylor series. Equation 6 can be further expressed as

$$\begin{aligned} \Delta\lambda_B &= \lambda_B(\phi_1 n_b, \phi_2 n_{sp}) - \lambda_B(\phi_1 n_{b0}, \phi_2 n_{sp0}) \\ &= \left(\phi_1 \Delta n_b \frac{\partial}{\partial n_b} + \phi_2 \Delta n_{sp} \frac{\partial}{\partial n_{sp}}\right)\lambda_B \end{aligned} \quad (7)$$

Furthermore, the relationship between the RI and the concentrations of the pure components in the mixture solution is assumed to satisfy the function equation

$$n_i = a_i C_i + b_i, \ (i = b, sp) \quad (8)$$

where a_i and b_i are constant parameters, and C_b and C_{sp} are the biomass and liquid-phase concentration of the bacterial suspension, respectively. Thus, by using eqs 7 and 8, the change in the wavelength with changes in the biomass and liquid-phase concentration can be expressed as

$$\Delta\lambda_B = \Delta C_b \cdot K_b + \Delta C_{sp} \cdot K_{sp} \quad (9)$$

where $K_b = \varphi_1 a_b(\partial\lambda_B/\partial\rho_b)$, $K_{sp} = \varphi_2 a_{sp}(\partial\lambda_B/\partial\rho_{sp})$, and K_b and K_{sp} represent the change in wavelength with changes in the biomass and liquid-phase concentration, respectively. Thus, the matrix can be expressed as

$$\begin{bmatrix} \Delta\lambda_{1B} \\ \Delta\lambda_{2B} \end{bmatrix} = \begin{bmatrix} k_{1b} & k_{1sp} \\ k_{2b} & k_{2sp} \end{bmatrix} \begin{bmatrix} \Delta C_b \\ \Delta C_{sp} \end{bmatrix} \quad (10)$$

One can see that matrix 10 can be used to separate the effects of the biomass and liquid phase on the wavelength change. Thus, in the experiments, the temperature and liquid-phase concentration information are first obtained using the MSFBG sensor, and then the biomass can be obtained using matrices 4, 5, and 10.

RESULTS AND DISCUSSION

For clarity, the unperturbed region, thinned region coated with PSHM, and the smaller thinned region of the proposed MSFBG sensor are denoted as FBG_A_3, FBG_A_2, and FBG_A_1, respectively, as mentioned in the Materials and Methods section.

Response Time. The Bragg resonance wavelength (central wavelength of the light back-reflected from the Bragg grating, λ_B) of a thinned-core FBG sensor can respond directly to the RI of the surrounding medium if we do not consider the effects of temperature and cell growth. The sensitivity of the sensor to the index of the surrounding medium depends entirely on the interaction of the evanescent field with the medium. However, for FBG_A_2, the response time and sensitivity will also be affected by the physical and chemical properties of the PSHM filter. To investigate the performance of FBG_A_2, we first investigate the response time and stability of the sensor with changes in the glucose concentration (RI). At 25 °C, FBG_A_2 was first immersed in distilled water for 10 min so that the membrane was fully swelled by the water, and then pulled out and inserted into a test tube containing a 3 g/100 mL glucose solution. When the rate of change of the wavelength ($\Delta\lambda_B$) reached equilibrium, the sensor was immediately inserted into another test tube of distilled water. A typical captured response is shown in Figure 4 (the sampling interval is 1 s). In all the experiments in this work, $\Delta\lambda_B$ represents the difference between the measured Bragg wavelength and the initial Bragg wavelength in distilled water at the same temperature for the proposed MSFBG sensor.

From the captured response, one can see that $\Delta\lambda_B$ varies significantly as a function of the glucose concentration (RI), because the RI of the region surrounding the thinned fiber depends on the diffusion rate of the glucose through the PSHM. The wavelength change increased with increasing time when the sensor was inserted into the glucose solution and thus decreased with increasing time when the glucose solution was replaced by distilled water, with response times of 255 and 397 s, respectively. Furthermore, the change in the wavelength initially increased rapidly when the sensor was inserted into and removed from the high-concentration glucose solution. The

dx.doi.org/10.1021/ac502417a | Anal. Chem. 2014, 86, 9278−9285

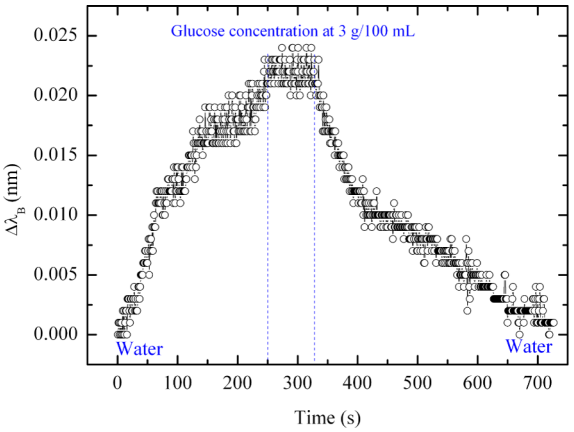

Figure 4. Response time of FBG_A_2.

reason is that the high glucose concentration builds a large concentration gradient between the bulk solution and the membrane, resulting in a high mass transfer rate. Thus, $\Delta\lambda_B$ changed rapidly. These facts show that the PSHM-coated FBG_A_2 can provide a reversible process and fast response to changes in the liquid-phase concentration.

Sensor Performance in Offline Measurement. To evaluate the sensitivity and feasibility of the proposed MSFBG sensor for accurate and simultaneous detection of the biomass and temperature, three types of experiments were conducted to investigate the Bragg wavelength changes with changes in the temperature, biomass, and glucose concentration. The sensor performance in offline measurements are described in section S1 of the Supporting Information. According to the offline measurements results (Figures S1–S3) as shown in the section S1 of the Supporting Information, the matrices can be obtained directly from the experimental data with linear fits using matrices 4, 5, and 10, as follows:

$$\begin{bmatrix}\Delta\lambda_{B,2}\\ \Delta\lambda_{B,3}\end{bmatrix}=\begin{bmatrix}k_{2x} & k_{2t}\\ k_{3x} & k_{3t}\end{bmatrix}\begin{bmatrix}\Delta x\\ \Delta t\end{bmatrix}=\begin{bmatrix}0.0075 & 0.0093\\ 0 & 0.0098\end{bmatrix}\begin{bmatrix}\Delta x\\ \Delta t\end{bmatrix} \tag{11}$$

$$\begin{bmatrix}\Delta\lambda_{B,1}\\ \Delta\lambda_{B,3}\end{bmatrix}=\begin{bmatrix}k_{1y} & k_{1t}\\ k_{3y} & k_{3t}\end{bmatrix}\begin{bmatrix}\Delta y\\ \Delta t\end{bmatrix}=\begin{bmatrix}0.7617 & 0.0087\\ 0 & 0.0098\end{bmatrix}\begin{bmatrix}\Delta y\\ \Delta t\end{bmatrix} \tag{12}$$

$$\begin{aligned}\begin{bmatrix}\Delta\lambda_{1B}\\ \Delta\lambda_{2B}\end{bmatrix}&=\begin{bmatrix}k_{1b} & k_{1sp}\\ k_{2b} & k_{2sp}\end{bmatrix}\begin{bmatrix}\Delta C_b\\ \Delta C_{sp}\end{bmatrix}\\ &=\begin{bmatrix}\dfrac{\sum_{i=1}^{N}(\Delta\lambda_{1B,i}-1.5467k_{2sp}\Delta C_{sp,i})}{N} & 1.5467k_{2sp}\\ 0 & k_{2sp}\end{bmatrix}\begin{bmatrix}\Delta C_b\\ \Delta C_{sp}\end{bmatrix}\\ &=\begin{bmatrix}0.2717 & 0.6143\\ 0 & 0.3972\end{bmatrix}\begin{bmatrix}\Delta C_b\\ \Delta C_{sp}\end{bmatrix}\end{aligned} \tag{13}$$

where N is the number of samples, the wavelength change is in nanometers, the biomass and glucose concentration are both in g/100 mL, and the temperature is in degrees centigrade. The available matrices can yield simultaneous accurate measurements of the biomass, temperature, and liquid concentration. However, these established matrices were obtained from the offline experimental results. In the actual bacterial culture process, not only the biomass and temperature but also the temperature, composition, and concentration of the liquid phase will change. Thus, to further validate the feasibility of the proposed FBG sensor for simultaneous monitoring of the biomass concentration and temperature, online measurement of a cell culture is necessary.

Online Monitoring of PSB Culture. The experimental systems for the online MSFBG sensor and photobioreactor are shown in Figure 3. Before the experiment, 21 mL of a prepared suspension of the PSB CQK 01 (5 °C) was injected into the bioreactor with 210 mL of fresh culture medium (25 °C) with an initial biomass concentration of 0.013 g/100 mL, and the initial pH value of the medium was adjusted to 7.0 using 0.1 M NaOH. The sampling interval was 150 s during the online measurement. The ambient temperature was controlled only by the room air conditioner. Furthermore, to investigate the metabolic heat production in the cell culture, the reference temperature in 250 mL Buchner flasks filled with 21 or 210 mL of fresh culture medium at temperatures of 5 or 25 °C was also measured using a normal FBG sensor (FBG_A_4) with a central wavelength of 1530.154 nm [$\Delta\lambda_{B4} = 0.0098t - 0.1827$ (R^2 = 0.9994), where t denotes the temperature, °C]. The change in the Bragg wavelength, $\Delta\lambda_B$, of the MSFBG sensor with the cell culture time, the $\Delta\lambda_B$ value of FBG_A_4, and the actual biomass (biomass dry weight) are shown in Figure 5a.

The $\Delta\lambda_B$ values for the MSFBG sensor and FBG_A_4 increased significantly in the first 3 h. This can be attributed to the fact that the temperature in the reactor was lower than the ambient temperature because of the addition of the low-temperature seed suspension or fresh culture medium (5 °C). Thus, $\Delta\lambda_B$ increased with increasing temperature. Thereafter, $\Delta\lambda_B$ fluctuated with increasing time when the temperature in the bioreactors was raised to the ambient temperature. This can be explained as follows. (1) The ambient temperature is different in the day and at night. (2) For the MSFBG sensor (FBG_A_1, FBG_A_2, and FBG_A_3), the changes were affected by the metabolic heat production of the cell. (3) For FBG_A_1 and FBG_A_2, $\Delta\lambda_B$ was also affected by the change in the substrate–product concentration. (4) For FBG_A_1, $\Delta\lambda_B$ was further affected by the change in the biomass. Thus, it is very important to distinguish and reveal the effects of the various factors on the output of the entire sensor.

To clearly distinguish the effects of the various factors on the output of the entire sensor, the original data were processed as follows. (1) The temperature difference between the photobioreactor and the Buchner flask without cells was calculated from the obtained formulas [$\Delta\lambda_{B4} = 0.0098t - 0.1827$, $\Delta\lambda_{B3} = 0.0098t - 0.2069$ (Figure S1 in the section S1 of the Supporting Information), where t denotes the temperature, °C], as we know that the temperature difference arises from metabolic heat production. The calculated results are shown in Figure 5b. (2) The available information, including the mixture concentration (i.e., biomass and liquid phase) and temperature, was separated from the original data (Figure 5a) using the second-order matrices 11 and 12. Using the separated information, the contribution of the liquid concentration to the change in wavelength for FBG_A_1 can be obtained using

dx.doi.org/10.1021/ac502417a | Anal. Chem. 2014, 86, 9278–9285

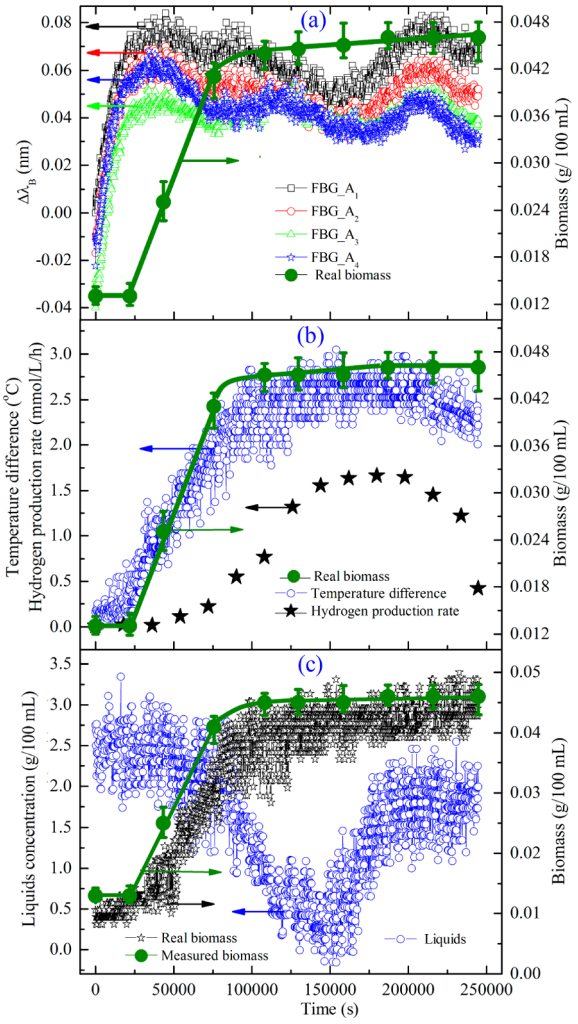

Figure 5. (a) Output signal of MSFBG sensor and actual biomass as a function of culture time; (b) temperature difference (metabolic heat production) and actual biomass as a function of culture time; (c) measured data (liquid concentration and biomass) and actual biomass as a function of culture time.

matrix 13; the obtained biomass and liquid-phase concentration are shown in Figure 5c.

Figure 5b shows that the temperature difference experienced four phases: a stable phase, fast increase phase, stationary phase, and decrease phase. The first three phases are the same as those in the PSB CQK 01 cell growth curve (the real biomass as shown in Figure 5, the error bars show the standard deviation of three repeated measurements of each sample), and a maximum temperature difference of 2.8 °C appeared at a culture time of about 60 h. However, the temperature difference subsequently decreased with increasing culture time, even though the biomass remained in the stationary phase (0.046 g/100 mL). This can be explained by the facts that the cell activity and metabolic heat production decrease because of product inhibition, limited light energy, and an inadequate substrate supply (Figure 5c). Furthermore, Figure 5b shows that the hydrogen production rate of the bioreactor also experienced four phases, as indicated by the changes in the temperature difference in the culture. The highest hydrogen production rate, 1.97 mmol/L/h, was obtained at about 60 h; thereafter, the rate decreased with increasing culture time, decreasing quickly when the time was greater than 70 h. These facts show that the cell metabolic activity and hydrogen production capacity were gradually inhibited after 60 h. Thus, in the experiment, the temperature difference (i.e., metabolic heat production) can be used as a proof-of-principle assay to reflect the cell activity in a culture.

In Figure 5c, the amount of change in the liquid concentration (ΔC_{sp}) of the PSB suspension first remains high because the synthetic medium is not consumed early in the cell culture process (the biomass remained at a low level of 0.013 g/100 mL, i.e., the lag phase). Thereafter, ΔC_{sp} decreased rapidly with increasing culture time. This fact can be explained as follows: the cells entered the exponential phase and reached a high concentration (0.045 g/100 mL), leading to rapid consumption of the substrate. The substrate consumption rate exceeded the production rate of small molecular organic acids in the early phase of cell growth because most of the substrate was used for the propagation of cells,[33] metabolic heat, and H_2 and CO_2 production, and only a small part of it was metabolized into organic acids. Thus, the ΔC_{sp} value of the bacterial suspension decreased. However, ΔC_{sp} increased after 52 h. This increase can be attributed to an increase in the number of metabolic components and their concentration[34] because PSB growth and hydrogen production were inhibited by substrate scarcity in the fermentation environment (the glucose concentration was below 0.05 g/L after 52 h), limiting the bacterial metabolic pathways and leading to the accumulation of organic acids..[35] Hence, ΔC_{sp} increased with increasing culture time. The decreases in the cell activity and metabolic heat production further explain the decrease in the temperature difference with increasing culture time after 60 h (Figure 5b).

The amount of change in biomass ΔC_b, shown in Figure 5c, remained at a low constant level for the first 8 h and then increased significantly between 8 and 52 h; thereafter, it again remained constant at a high level. The fact is fully consistent with the bacterial growth curve; i.e., the cell growth experienced three phases: a lag phase, logarithmic phase, and stationary phase. For the lag phase (first 8 h), the PSB cells were not activated; when the PSB strain entered the logarithmic growth phase, the biomass increased rapidly. Thereafter, the cells almost ceased to grow, and ΔC_b once again remained constant.

To analyze the accuracy of the biomass measurement, we use the correlation degree of the biomass measured using the proposed sensor and the actual biomass (Figure 5c) based on the gray absolute correlation degree (absolute degree of gray incidence, ADGI).[36] The ADGI and data evaluation algorithms are described in detail in section S2 of the Supporting Information. According to the calculations, we obtained an absolute correlation degree of 0.9438 between the curves of the measured and actual biomass in Figure 5c. The high correlation degree means that the changes in the curves are in agreement during the PSB CQK 01 culture process. These facts demonstrate that the proposed MSFBG sensor can be used to accurately and simultaneously monitor the biomass and temperature in the cell culture.

SUMMARY

A low-cost MSFBG sensor based on a normal FBG unit demonstrated accurate simultaneous measurement of biomass and temperature. The proposed MSFBG sensor consisted of an unperturbed grating region that is sensitive to temperature, a PSHM-coated thinned grating region (diameter, 7.1 μm) that is sensitive to the liquid concentration and temperature of a

dx.doi.org/10.1021/ac502417a | Anal. Chem. 2014, 86, 9278−9285

bacterial suspension, and another thinned grating (diameter, 4.5 μm) that was used to monitor the biomass, liquid-phase concentration, and temperature. We also developed two models to demonstrate accurate simultaneous measurement of the biomass and temperature by the proposed sensor. The experimental results showed that the PSHM-coated FBG region can respond rapidly (response time of less than 397 s) to changes in the solution concentration; the result of online biomass measurement exhibits a high correlation degree (0.9438) with the real biomass from the lag phase to the stable phase in a PSB culture. We also discovered that the temperature difference due to metabolic heat production and the hydrogen production rate reached 2.8 °C and 1.97 mmol/L/h, respectively, in the stable phase. In conclusion, the proposed sensor can be used to accurately and simultaneously monitor the biomass, liquid concentration, and temperature, and it can also be applied in other fields, including chemistry, biochemistry, the life sciences, and the environmental sciences.

■ ASSOCIATED CONTENT

Supporting Information

Additional materials as described in the text. This material is available free of charge via the Internet at http://pubs.acs.org/.

■ AUTHOR INFORMATION

Corresponding Authors

*Tel.:+86-023-62563277, Fax: +86-023-62563277. E-mail: zhongnianbing@163.com.

*E-mail: lqzx@cqu.edu.cn.

Notes

The authors declare no competing financial interest.

■ ACKNOWLEDGMENTS

This work was supported by the National Natural Science Foundation of China (No. 51406020; No. 51276209) and the Key Projects of the National Natural Science Foundation of China (No. 51136007).

■ REFERENCES

(1) Märk, J.; Karner, M.; Andre, M.; Rueland, J.; Huck, W. C. *Anal. Chem.* **2010**, *82*, 4209.

(2) Brkic, B.; France, N.; Taylor, S. *Anal. Chem.* **2011**, *83*, 6230.

(3) Liu, W. J.; Ma, C. Y.; Feng, S. X.; Wang, Z. X. *J. Chem. Eng. Data* **2014**, *59*, 807.

(4) Philip-Chandy, R.; Scully, P. J.; Eldridge, P.; Kadim, H. J.; Grapin, M. G.; Jonca, M. G.; D'Ambrosio, M. G.; Colin, F. *IEEE J. Sel. Top. Quantum Electron.* **2000**, *6*, 764.

(5) Monlau, F.; Trably, E.; Barakat, A.; Hamelin, J.; Steyer, J. P.; Carrere, H. *Environ. Sci. Technol.* **2013**, *47*, 12591.

(6) Bradley, S. A.; Ouyang, A.; Purdie, J.; Smitka, T. A.; Wang, T. T.; Kaerner, A. *J. Am. Chem. Soc.* **2010**, *132*, 9531.

(7) Dandoy, P.; Danloy, E.; Leroux, G.; Meunier, C. F.; Rooke, J. C.; Su, B. L. *Chem. Soc. Rev.* **2011**, *40*, 860.

(8) Mahfoud, C.; El Samrani, A.; Mouawad, R.; Hleihel, W.; El Khatib, R.; Lartiges, B. S.; Ouaïni, N. *J. Environ. Sci.* **2009**, *21*, 120.

(9) Zhu, X.; Guo, C. L.; Wang, Y. Z.; Liao, Q.; Chen, R.; Lee, D. J. *Int. J. Hydrogen Energy* **2012**, *37*, 15666.

(10) Zhong, N. B.; Liao, Q.; Zhu, X.; Chen, R. *Anal. Chem.* **2014**, *86*, 3994.

(11) Argun, H.; Kargi, F. *Int. J. Hydrogen Energy* **2011**, *36*, 7443.

(12) Kargi, F.; Eren, N. S.; Ozmihci, S. *Biotechnol. Prog.* **2012**, *28*, 931.

(13) Liao, Q.; Qu, X. F.; Chen, R.; Wang, Y. Z.; Zhu, X.; Lee, D. J. *Int. J. Hydrogen Energy* **2012**, *37*, 15443.

(14) Lee, S. J.; Kenyon, C. *Curr. Biol.* **2009**, *19*, 715.

(15) Dijkstra, P.; Thomas, S. C.; Heinrich, P. L.; Koch, G. W.; Schwartz, E.; Hungate, B. A. *Soil. Biol. Biochem.* **2011**, *43*, 2023.

(16) Ge, Z.; Cavinato, A. G.; Callis, J. B. *Anal. Chem.* **1994**, *66*, 1354.

(17) Griffiths, M. J.; Garcin, C.; van Hille, R. P.; Harrison, S. T. L. *J. Microbiol. Meth.* **2011**, *85*, 119.

(18) Beuermann, T.; Egly, D.; Geoerg, D.; Klug, K. I.; Storhas, W.; Methner, F. J. *J. Biosci. Bioeng.* **2012**, *113*, 399.

(19) Keskar, S. S.; Edye, L. A.; Fellows, C. M.; Doherty, W. O. S. *J. Wood. Chem. Technol.* **2012**, *32*, 175.

(20) Pereira, D. A.; Santos, J. L.; Frazão, O. *Opt. Eng.* **2004**, *43*, 299.

(21) Cao, Y.; Yang, Y. F.; Yang, X. F.; Tong, Z. R. *Chin. Opt. Lett.* **2012**, *10*, 030605.

(22) Liang, W.; Huang, Y. Y.; Xu, Y.; Lee, R. K.; Yariv, A. *Appl. Phys. Lett.* **2005**, *86*, 151122.

(23) Saffari, P.; Yan, Z. J.; Zhou, K. M.; Zhang, L. *Appl. Opt.* **2012**, *51*, 4715.

(24) Zhong, N. B.; Zhu, X.; Liao, Q.; Wang, Y. Z.; Chen, R.; Sun, Y. F. *Appl. Opt.* **2013**, *52*, 3937.

(25) Zhong, N. B.; Liao, Q.; Zhu, X.; Wang, Y. Z.; Chen, R. *Appl. Opt.* **2013**, *52*, 1432.

(26) Zhong, N. B.; Liao, Q.; Zhu, X.; Wang, Y. Z.; Chen, R. *Opt. Precis. Eng.* **2012**, *20*, 988.

(27) Chang, C. C.; Chen, W. C. *Chem. Mater.* **2002**, *14*, 4242.

(28) Melis, C.; Mattoni, A.; Colombo, L. J. *Phys. Chem. C* **2010**, *114*, 3401.

(29) Zhong, S. H.; Li, C. F.; Xiao, X. F. *J. Membr. Sci.* **2002**, *199*, 53.

(30) Qian, J. C.; Chen, F.; Wang, F.; Zhao, X. B.; Chen, Z. G. *Mater. Res. Bull.* **2012**, *47*, 1845.

(31) Iadicicco, A.; Campopiano, S.; Cutolo, A. *IEEE Photonics Technol. Lett.* **2005**, *17*, 1495.

(32) Wiederseiner, S.; Andreini, N.; Epely-Chauvin, G.; Ancey, C. *Exp. Fluids* **2011**, *50*, 1183.

(33) Schiff, R. D.; Grandgenett, D. P. *J. Virol.* **1978**, *28*, 279.

(34) Chin, H. L.; Chen, Z. S.; Chou, C. P. *Biotechnol. Prog.* **2003**, *19*, 383.

(35) Hadi, T. A.; Banerjee, R.; Bhattacharyya, B. C. *Bioprocess Eng.* **1994**, *11*, 239.

(36) Tung, C. T.; Lee, Y. J. *Expert Syst. Appl.* **2010**, *37*, 7844.